Medical Engineering and Physics 135 (2025) 104274

Contents lists available at ScienceDirect

Medical Engineering and Physics

journal homepage: www.elsevier.com/locate/medengphy

# A finite element model to simulate intraoperative fractures in cementless hip stem designs

Maila Petrucci [a,b], Antonino A. La Mattina [a], Cristina Curreli [a], Enrico Tassinari [c], Marco Viceconti [a,b,*]

[a] Medical Technology Lab, IRCCS Istituto Ortopedico Rizzoli, Bologna, Italy
[b] Department of Industrial Engineering, Alma Mater Studiorum - University of Bologna, Italy
[c] Orthopaedic-Traumatology and Prosthetic surgery and revisions of hip and knee implants, IRCCS Istituto Ortopedico Rizzoli, Bologna, Italy

ARTICLE INFO

*Keywords:*
Cementless hip stem
Patient-specific finite element model
Intraoperative femur fracture
Crack propagation
Elements deactivation
In silico trials

ABSTRACT

Intraoperative femur fractures are a complication of hip arthroplasty, strongly related to the cementless stem design; this kind of fracture is not always recognised during surgery, and revision surgery may be necessary. The present study aimed to simulate intraoperative crack propagation during stem implantation using subject-specific quasi-static finite element models. Eleven subject-specific finite element femur models were built starting from CT data, and the implant pose and size of a non-commercial cementless stem were identified. The model boundary conditions were set with a compressive load from 1000 N to 10 000 N, to simulate the surgeon's hammering, and element deactivation was used to model the crack propagation. Two damage quantifiers were analysed to identify a threshold value that would allow us to assess if a fracture occurred. A methodology to assess the primary stability of the stem during insertion was also proposed, based on a push-out test. Crack propagation up to the surface was obtained in six patients; in two cases there was no crack generation, while in three patients the crack did not reach the external surface. This study demonstrates the possibility to simulate the propagation of the fracture intraoperatively during hip replacement surgery and generate quantitative information about the bone damage using a virtual cohort of simulated patients with anatomical and physiological variability.

## 1. Introduction

Total hip arthroplasty (THA) is a widely adopted solution to restore joint motion and alleviate severe pain at the hip joint resulting from musculoskeletal disorders (*e.g.*, inflammatory arthritis, osteoporosis, osteoarthritis). According to THA outcome registries, more than one million THAs are performed every year around the world [1], and by 2030 the demand is expected to drastically increase (almost doubling from 2005), mainly due to the ageing population [2,3]. In Italy, one of the countries with the oldest population, the Italian Arthroplasty Registry (RIAP) reported approximately 80 000 hip replacement surgeries in 2019, an increase of 5.7 % compared to 2018 [4].

Although THA represents one of the most successful and frequent orthopaedic procedures, with an overall survival rate higher than 95 % at ten-year follow-up [5], the number of revisions is constantly increasing as a result of the increase in both life expectancy and the number of non-elderly (and physically active) patients (35 % of all THA patients are younger than 65 years, with an expected growth of 50 % by 2030) [6]. Consequently, improving surgical techniques and technologies has been and is still necessary to develop new, less invasive, and longer-surviving implants. While the most common reasons for THA failure are aseptic loosening, infection, and repeated dislocation, the frequent use of cementless implants increased the probability that an intraoperative femur fracture (IFF) occurs (approximately 3–5 % of all cementless total hip arthroplasty surgeries) [3]. Intraoperative fractures extend the surgical procedure time and frequently require revision surgery, possibly delaying recovery after the initial operation [7]. But what is most concerning is that the incidence of this complication seems to vary considerably depending on the design of the cementless stem. For example, the Regional Register of the Orthopaedic Prosthetic Implants (RIPO, hosted by Rizzoli Orthopaedic Institute) reports a prevalence of IFF of just 0.4 % for the Zimmer-Biomet Avenir Muller stem and of 4 % for the Zimmer-Biomet Mayo stem. Other studies report similar or higher IFF incidences for the Mayo stem (4.2 % according to Rutenberg

* Corresponding author at: Dept. di Industrial Engineering, Alma Mater Studiorum – University of Bologna, Via Terracini 24, 40131 Bologna, Italy.
*E-mail address:* marco.viceconti@unibo.it (M. Viceconti).

https://doi.org/10.1016/j.medengphy.2024.104274
Received 31 January 2024; Received in revised form 11 November 2024; Accepted 1 December 2024
Available online 2 December 2024

et al. [6] and 12.1 % according to Arnholdt et al. [8]).

The risk of IFF has been analysed through *in vitro* experiments to understand the mechanical behaviour of the femur during stem implantation and to explore parameters that influence the surgical outcome, such as force, frequency and number of hammer strokes [9–13]. However, the destructive nature of these experiments makes it difficult to systematically compare different designs, given that the risk of IFF depends as much on the femoral anatomy than it does on the stem design. Numerical simulation studies could explore how two different designs perform in terms of IFF risk in the same femoral anatomy; however, there are very few computational studies on this topic in the literature. The most common approach to simulate the IFF scenario is to use transient Finite Element (FE) models for dynamic analysis to observe the evolution of contact surfaces, stress and strain distributions during cementless stem insertion. In these models, the maximum stress values in cancellous bone are used as local failure criterion [14–16]. However, such complex constitutive equations require the identification of patient-specific parameters, which are difficult to quantify in most cases. Some authors focus on the periprosthetic fracture risk in the early postoperative period: Saemann et al. modelled bone as an elastic, perfectly plastic material [17], assuming fracture when an element reached yield strain; on the other hand, Miles et al. simulated both the initiation and propagation of the crack using element deactivation technique [18]. Marco *et al.* compared different FE modelling techniques to predict realistic femur fracture paths in the proximal femur during stance and sideways fall loading conditions [19]. They concluded that the eXtended Finite Element Method (XFEM) could be used to simulate the initial steps of crack propagation. At the same time, the material property degradation technique yielded the best results for long fracture growth, as it provided a closer match between experimental and numerical fracture patterns. More recently, an Incremental Element Deletion-Based FE analysis was used to predict femur fracture trajectories under various post-operative loading scenarios [20]. This study suggests using this approach to estimate the risk of IFF.

The present study aims to describe a new approach to simulate intraoperative crack propagation using a simple quasi-static FE model identified using only clinically measurable information. Some degrees of idealisation, as explained in the materials and methods section, have been introduced to reduce computational cost. Moreover, possible damage quantifiers were investigated to detect threshold values that would allow an automatic prediction of the moment the crack reached a depth at which the femur could be considered fractured.

To describe the methodology in detail, a non-commercial, copyright-free design of a cementless stem was used; this will enable sharing of all simulation data in Open Access, simplifying future benchmarking comparisons by other research groups.

## 2. Materials and methods

### 2.1. Generation of the virtual cohort

To simulate intra-operative fracture for a given cementless stem design, we need to create a virtual cohort that captures all the variables that influence the risk of IFF. These include anatomical, densitometric, and surgical variables.

#### 2.1.1. Anatomical and densitometric variability

The inter-subject anatomo-densitometric variability was captured using the HipOp collection at the Rizzoli Orthopaedic Institute. The collection includes over 4000 calibrated CT scans of the hip region, originally collected for computer-aided preoperative planning of total hip replacements. First, we selected 500 scans of deceased patients. At the time of examination, patients had provided a pre-GDPR informed consent, which authorised the secondary use of their clinical data for research purposes; however, being deceased makes the legal basis for sharing their clinical data in an irreversibly anonymised form more robust.

From this cohort of 500 patients, we excluded cases with previous metal implants (which would cause metal artefacts) and cases with hip dysplasia or other skeletal deformities. From the remaining cases, we selected the CT scans of eleven patients, who were chosen because they represented, within the cohort, extreme values in terms of the four most important determinants for bone strength: age, gender, size (estimated with the femoral biomechanical length), and degree of osteoporosis. The biomechanical length was measured as the distance between the centre of a sphere fitting the femoral head and the midpoint of the line connecting the medial and lateral knee epicondyles. Since all the CT datasets were density-calibrated, we used volumetric Bone Mineral Density (vBMD) to evaluate the degree of osteoporosis. We also used a virtual DXA algorithm similar to that described in [21] to estimate the T-score [22].

For each gender group, we selected the patients with the shortest and longest biomechanical lengths. Then, we selected the group's youngest and oldest, and one (female) with a reported fragility fracture within five years after the CT scan. Lastly, we also selected a patient with both average age and femur length for each group, for a total of five male and six female patients. This selection was necessary to have a representative population and consider the patient anatomical variability. The main characteristics of the selected eleven patients are summarised in Table 1.

To further expand the densitometric variability, we uniformly scaled the cortical bone mineral density, thus producing a total of 33 virtual patients. A +/- 5% variation in areal bone mineral density, corresponding to more than five years [24], was considered. A preliminary study [23] investigated phenomenologically the volumetric bone mineral density in the proximal femur spongious and cortical components with respect to the total proximal femur areal bone mineral density in 98 post-menopausal women. By incorporating these results in the density-stiffness empirical law (see section "Finite element modelling and simulation"), we obtained that a 5% variation in proximal femur BMD corresponds to approximately a 3% variation in cortical elastic modulus.

Considering that, as shown in the results section, the variation of the elastic modulus (E) did not affect the results in a significant way, post-processing analyses for the damage quantification were performed only on the eleven original model densities.

#### 2.1.2. Surgical variability

To make all the results of this study freely accessible, we used a non-commercial cementless hip stem ("hip" model) downloaded from the GrabCAD website [25]. The corresponding rasp model, necessary to reproduce reaming operations, was generated by adding a cylinder at the apex of the stem and an extrusion on the proximal part (Fig. 1a). Eventually, three different implant sizes were considered (Table 1): Size 1 and 2 were generated (MeshLab, v 2020.02 [26]) with an isometric uniform outward offset of 1 and 2 mm, respectively, compared to the original CAD size (Size 0). For each of the 11 selected patients, the size of the stem and its pose (position and orientation) inside the femur were defined by an expert orthopaedic surgeon using a CT-based pre-operative planning software (HipOp-Plan) [27]. As shown in Table 1, for female patients, all three available sizes were selected and implanted, whereas for male patients, the largest size (*i.e.,* size 2) was chosen for all five femurs.

The 3D shape of each femur was segmented from the CT scan by thresholding at HU = 200 (E ~ 1500 MPa) using a general-purpose image processing software (3D Slicer, v. 4.10.2), as reported in [28]. This approach excluded regions of cancellous bone with very low mineral density and high degree of porosity, that would cause convergence problems, but ensured, at the same time, a good contact surface with the prosthesis stem (Fig. 1b). By using the roto-translation matrix obtained from the surgeon pre-operative planning, the prosthetic components were positioned in the femoral geometry, the femoral neck was resected, and Boolean subtraction between bone and rasp model (with the same

**Table 1**
Summary of the selected patients' data. The implant size is also reported for each case.

| Patient | Gender | Age (y) | Height (cm) | Weight (kg) | Implanted side | Implant size | T-score* | Biomechanical length (mm) |
|---|---|---|---|---|---|---|---|---|
| **P01** | F | 41 | 163 | 80 | L | 1 | −0.82 | 371.63 |
| **P02** | F | 70 | N.A. | 69 | R | 2 | −0.88 | 366.19 |
| **P03** | M | 87 | 165 | 67 | R | 2 | −2.39 | 439.01 |
| **P04** | M | 39 | 190 | 107 | L | 2 | −1.77 | 469.51 |
| **P05** | F | 77 | 134 | 55 | L | 0 | −1.54 | 334.20 |
| **P06** | F | 76 | 168 | 100 | L | 1 | −2.07 | 419.85 |
| **P07** | F | 84 | 150 | 64 | L | 2 | −2.31 | 361.51 |
| **P08** | M | 49 | 166 | 93 | L | 2 | 0.51 | 374.42 |
| **P09** | F | 75 | 160 | 160 | R | 2 | −1.83 | 384.33 |
| **P10** | M | 67 | 164 | 72 | R | 2 | +1.06 | 393.52 |
| **P11** | M | 53 | 187 | 88 | R | 2 | +0.02 | 465.19 |

* Virtual DXA using NHANES III reference data [22], adjusted for sex.

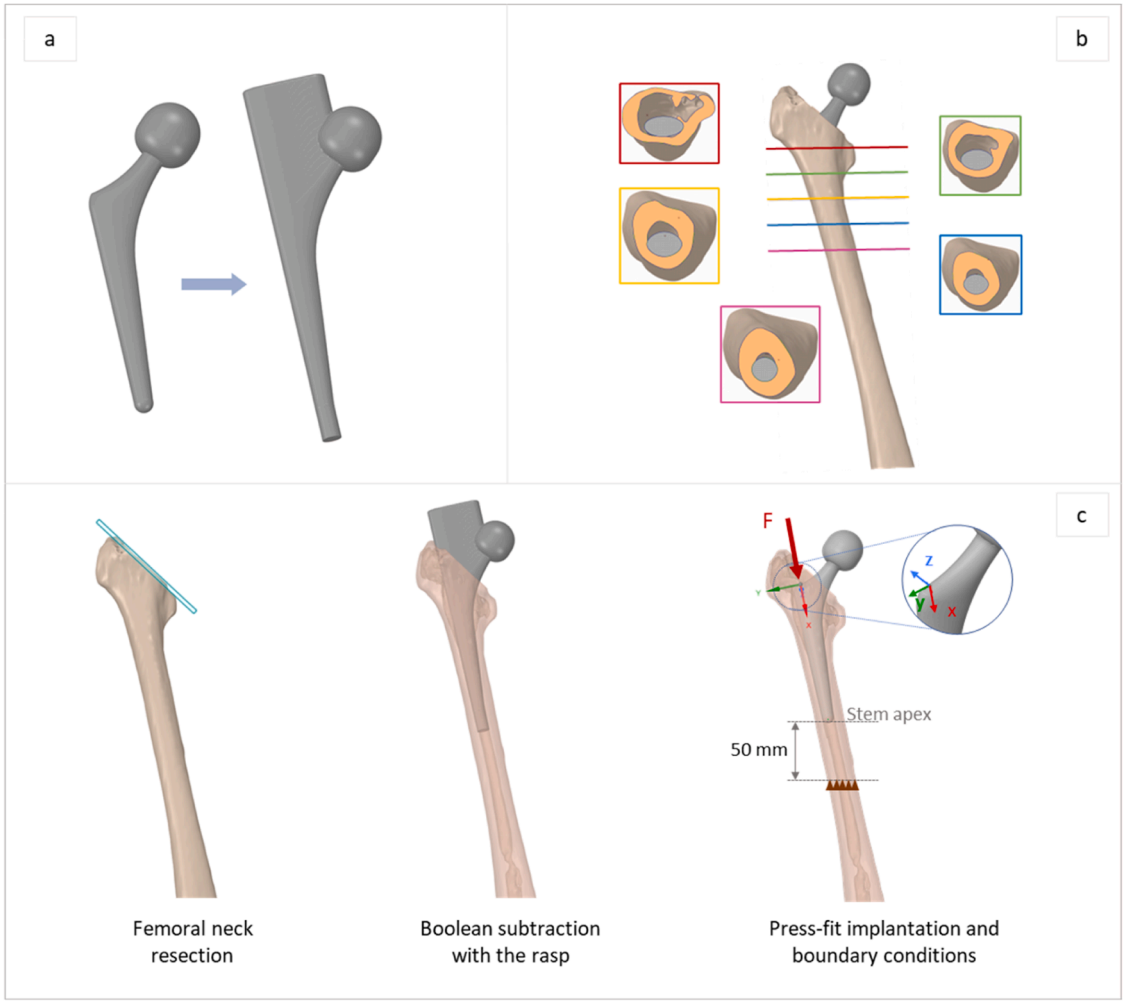


**Fig. 1.** a) Stem CAD model (on the left) and the derived rasp geometry (on the right), necessary to reproduce the reaming procedure; b) Axial sections of the femur diaphysis showing the contact between the threshold-segmented bone and the stem at different levels; c) Main steps of the model generation; in detail, the defined local reference system and the applied boundary conditions.

size as the selected stem) was performed using a 3D modelling software (SpaceClaim v. 2019R3, Ansys Inc., Canonsburg, PA).

### 2.2. *Finite element modelling and simulation*

For each of the 33 cases, the femur and stem models were meshed with 10-node quadratic tetrahedral elements with 2 mm max edge length using Ansys ICEM CFD (2019R3, Ansys Inc.) [29,30]; a curvature/proximity-based refinement with a minimum element size limit of 1 mm was added to accurately reproduce the contact surface geometries. Bone was modelled as a heterogeneous linear elastic material in which properties were assigned element-wise using Bonemat software (Bonemat V3.1, Istituto Ortopedico Rizzoli, Bologna, Italy) depending on local mineral density estimated from the calibrated CT

scan of the patient [31–33]. In particular, at each element of the mesh was first assigned a volumetric bone mineral density ($\rho_{QCT}$) value derived from the HU values using a linear calibration from ESP phantom offline scans:

$$\rho_{QCT} = a + b * HU \quad (1)$$

where the values of $a$ and $b$ depended on the scan. The density to elasticity relationships (Eqs (2) and (3) were used to convert $\rho_{QCT}$ to ash density ($\rho_{ash}$) [31,33] and subsequently to the elastic modulus ($E$), assuming $\rho_{app} = \rho_{ash}/0.6$ [31].

$$\rho_{ash} = 0.079 + 0.8772 * \rho_{QCT} \quad (2)$$

$$E = 14664 * \rho_{ash}^{1.49} \quad (3)$$

The cementless stem was assumed to be made of a Titanium Alloy ($E$ = 105 GPa, $\nu$ = 0.3) with a linear elastic behaviour [34]. The bone–implant interface was modelled with an asymmetric (stem as target, femur as contact) face-to-face large-sliding frictional contact ($\mu$ = 0.3 [34]) in Ansys Mechanical APDL (2019R3, Ansys Inc.), assuming no initial interference fit.

A local reference system aligned with the stem shaft was used to define the loading condition, which replicated the force applied to the stem by the impactor during press-fit. The reference system was defined with the origin in a central and lateral point of the stem, the X-axis connecting the origin of the reference system with the stem distal apex centre, the Y-axis pointing toward the greater trochanter, and the Z-axis approximatively in the anteroposterior direction (Fig. 1c).

In all models, the femur was constrained with a fixed support 50 mm below the stem apex, as reported in previous studies [9,10,15]. Even if this approach drastically simplified the real condition, we ensured that Saint Venant's principle was verified. A quasi-static nodal compressive load was applied to the stem at the local reference system origin along its X-axis to reproduce the hammering stroke (Fig. 1c). The force magnitude was progressively increased to 10 000 N (about two times the hammering stroke, which, according to literature, produces a force of approximately 4000 N [11,13]) considering a loading step function with increments of 1000 N (Fig. 2a).

An element deactivation technique was adopted to simulate the crack propagation, considering a failure criterion based on the first principal strain, assuming the bone would fracture as a brittle material with crack propagation dominated by mode I (opening). Among the several fracture criteria reported in the literature, it was decided to use this approach because strain-based fracture criteria are considered more accurate in capturing the onset of fracture as compared to stress-based criteria [18,35,36], but also because the limit value is independent of the bone density, which is not the case for stress-based criteria [37] and, as already said, assuming mostly mode I crack propagation, tensile principal strains are the most critical. Preliminary tests, in which both tensile and compressive strain limits (equal to 0.0073 and 0.0104, respectively) were considered, confirmed that the elements that exceeded the threshold were mostly subjected to tension. Among the few that yield primarily to compression, many of them also exhibited excessive strain under tension. Therefore, during each load step, only the first principal strain of each element was checked on the Volume of Interest (VOI), and the elements with a strain greater than $\varepsilon_{11}$=0.0073 [36] were '*killed*'. The VOI is identified as the entire femur component, from the top to 10 mm below the apex of the stem, so as to consider only elements in the region of interest and far enough from the boundary conditions. The 'KILL' command of Ansys Mechanical APDL de-activates the selected elements by attributing them a quasi-null elastic modulus (~ $10^{-6}$ MPa), thus preventing their mechanical participation in the subsequent loading phases. During each load step, the force was kept constant, and the test-and-kill process was repeated for $N$ substeps until no more elements reached the strain threshold value. A restart procedure that preserved the strains accumulated in the implanted femur was used for each iteration. The flowchart of the procedure used to simulate crack propagation based on the element deactivation technique is simplified in Fig. 2b

### 2.3. Crack propagation and damage quantification

The simulation results were analysed in terms of crack propagation and failure load (*i.e.*, the last applied force before the simulation stopped). Two candidate damage quantifiers were also investigated to potentially identify when a femur could be considered fractured:

1. the Fracture Internal Surface (FIS);
2. the percentage of killed Volume Ratio (VR);

To estimate the Fracture Internal Surface, free surface elements were generated in the post-processing phase of each substep to calculate the "Tot fem area", *i.e.*, the area of all the external surface elements of the intact femur (in blue, Fig. 3b), the "Live fem area", *i.e.*, the area of live

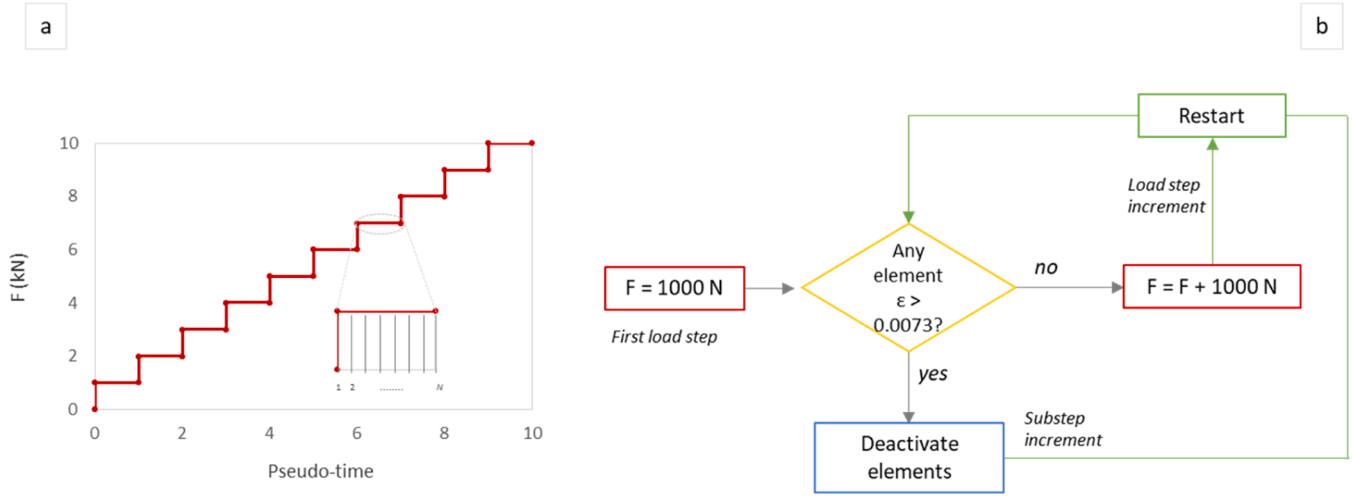


**Fig. 2.** a) Loading step function used to define the applied force magnitude (the number $N$ of substeps in each load step vary, depending on the test-and-kill process); b) Flowchart of the procedure used to simulate crack propagation based on the element deactivation technique.

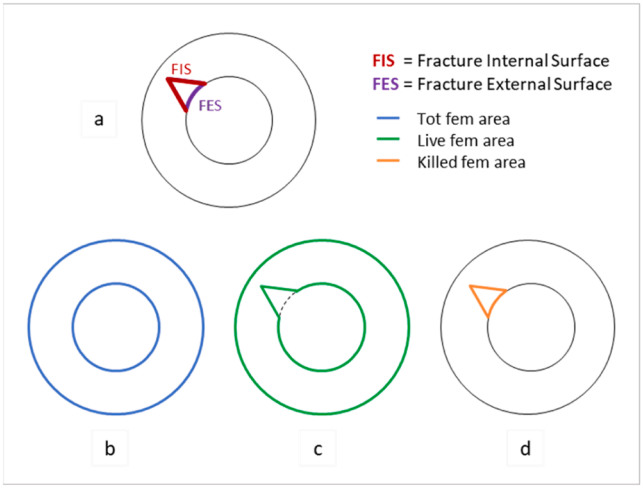


**Fig. 3.** a) Simplified scheme of a femur diaphysis section (inner and outer wall) with a crack started on the inside, where FES represents the crack surface at the femur surface, while FIS is the inner surface of the crack; b) Total (intact) femur element surface; c) Live femur element surface; d) Killed femur element surface.

(not killed) elements (in green, Fig. 3c), and the "Killed fem area", *i.e.*, the area of all solid killed elements (in orange, Fig. 3d).

Eventually, the FIS (Fig. 3a), namely the internal area of the crack, was calculated as:

$$\text{Fracture Internal Surface} = \left(\frac{\text{Live fem area} \; - - \; \text{Tot fem area} \; + \; \text{Killed fem area}}{2}\right) \tag{4}$$

as:

$$\text{Live fem area} = \text{Tot fem area} + \text{FIS} - \text{FES} \tag{5}$$

$$\text{Killed fem area} = \text{FIS} + \text{FES} \tag{6}$$

The killed Volume Ratio expressed the fraction of bone tissue inside the VOI that was cumulatively killed at each iteration. It was calculated as:

$$\text{Volume Ratio} = \left(\frac{\sum \text{volume killed elem}}{\sum \text{volume VOI elem}}\right) * 100 \tag{7}$$

VR was calculated at the end of each substep as well as FIS, before the restart.

### 2.4. Assessment of the primary stability of the stem

A methodology to assess the primary stability of the stem during insertion was also proposed, based on a push-out test. After each substep, the model was first unloaded, then a tensile load $F_{\text{push-out}}$ equal to 1000 N was applied to the same node of the compressive load along the X-axis of the local reference system shown in figure Fig. 1c. The push-out stiffness was computed as the ratio between the applied force and the difference in term of nodal displacement ($\Delta U_x$) computed at the pilot node at the end of the push-out test and at the end of the unloaded phase:

$$k_{\text{push-out}} = \frac{F_{\text{push-out}}}{\Delta U_x} \tag{8}$$

**Table 2**
Group classification of the simulation results based on crack propagation. The failure load is also reported for all the subjects analysed.

| Patient | Group | Failure Load (N) |
|---|---|---|
| **P01** | 1 | 10 000 |
| **P02** | 1 | 9000 |
| **P03** | 3 | 7000 |
| **P04** | 1 | 5000 |
| **P05** | 1 | 9000 |
| **P06** | 1 | 5000 |
| **P07** | 1 | 3000 |
| **P08** | 2 | >10 000 |
| **P09** | 3 | 7000 |
| **P10** | 2 | >10 000 |
| **P11** | 3 | >10 000 |

## 3. Results

### 3.1. Crack propagation

For all eleven models, the simulation stopped when the impact load reached the final imposed load of 10 000 N or as soon as the model became numerically unstable (*i.e.*, rigid-body motion caused by wide crack propagation or element distortion issues caused by the appearance of plastic hinges as the crack propagates). Analysing the crack propagation, we identified 3 macro-categories (Table 2):

1. Group 1: composed of six femurs, in which the crack propagated up to the external surface. Failure loads of 3000 N (P07), 5000 N (P04, P06), 9000 N (P02, P05), and 10 000 N (P01) were observed (Table 2). An example of the crack path for one subject from this group is depicted in Fig. 4a.
2. Group 2: composed of two femurs (P08, P10), where no crack was generated (*i.e.*, no elements were killed), and the simulation continued until the last imposed load (*i.e.*, $F = 10\,000$ N).
3. Group 3: composed of three femurs (P03, P09, P11), where the crack started but did not reach the external surface. An example of the crack path for one subject from this group is depicted in Fig. 4b. By analysing the results obtained, in all the three cases we observed element distortion issues which appeared to be caused by a structural failure due to crack propagation rather than original mesh-related problems.

### 3.2. Damage quantification

In order to quantify the bone damage, the Fracture Internal Surface and the killed Volume Ratio were calculated for all eleven models. The results obtained from this analysis were used to identify a threshold value that would allow predicting the moment the crack reached a depth level at which the femur could be considered fractured. Following visual inspection of the models (Fig. 5) and an empirical analysis of the results of the simulated models (Fig. 6), these threshold values have been identified around 1300 mm$^2$ for the FIS and 0.5 % for the VR, respectively. Notably, these values corresponded to cracks about halfway the femur cortical depth. In Fig 6(a-b), it can be observed that all the subjects in group 1 (*i.e.*, those with crack propagation up to the external surface) are above the thresholds at the end of the simulation, while those in group 2 (*i.e.*, with no crack propagation) are below the

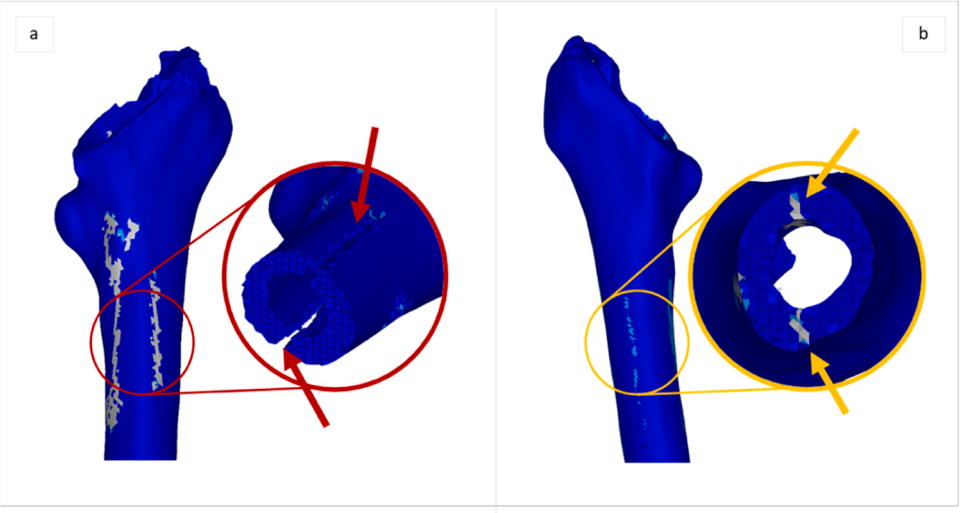


**Fig. 4.** a) Crack propagation up to the external surface. b) Crack starting but not propagating up to the surface due to excessive distortion of some elements. Killed elements are shown in gray to facilitate visual analysis. For simplicity, only the results obtained for cases P04 (on the left) and P09 (on the right) are reported.

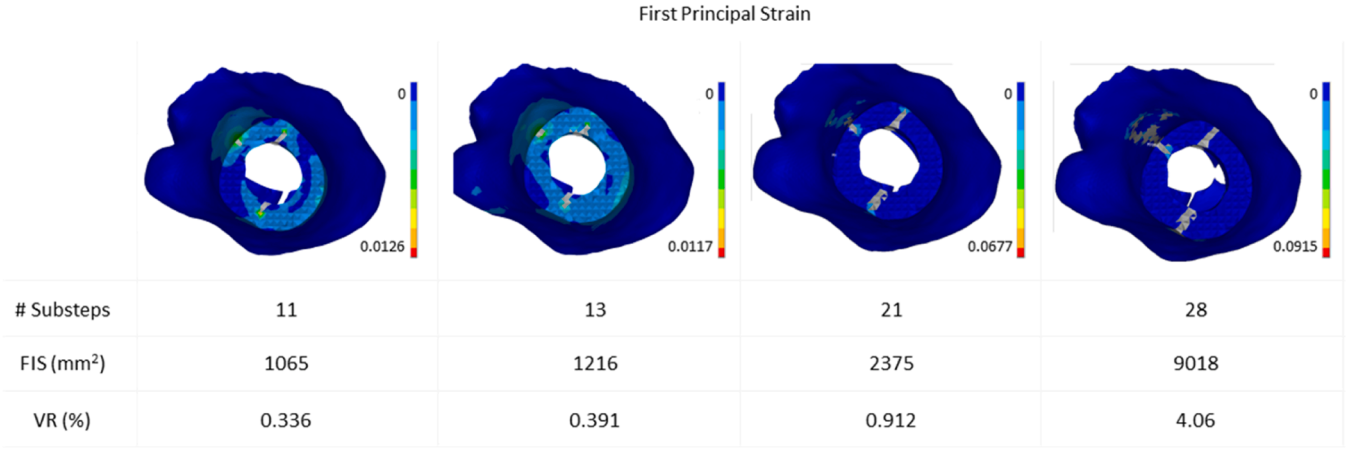


| | | | | |
|---|---|---|---|---|
| # Substeps | 11 | 13 | 21 | 28 |
| FIS (mm²) | 1065 | 1216 | 2375 | 9018 |
| VR (%) | 0.336 | 0.391 | 0.912 | 4.06 |

**Fig. 5.** Example of visual inspection performed on a cross-sectional area of P04 model during crack propagation. Results for First Principal Strain, FIS, and VR, extracted at different substeps of the final load step, are also reported.

thresholds. For the subjects in group 3, only P11, which indeed "resisted" the maximum applied load (*i.e.*, 10 000 N), did not reach the critical value for either quantity. In Fig 6c the relationship between the two damage quantifiers is also highlighted.

In Table 3, for the two damage quantifiers (*i.e.*, FIS and VR) it is reported the number *N* of substeps performed during the last load step if the simulation were terminated once the threshold value identified was achieved. Notably, the failure loads identified by FIS and VR were the same as those reported in Table 2 (*i.e.*, obtained when the simulation stopped because of as rigid-body motion or element distortion caused by crack propagation) in all the observed cases. Also, when considering only numerical instabilities as the stopping criterion, a higher number of substeps was needed (last column of Table 3), indicating that adopting the proposed damage quantification criteria could reduce the computational cost of the simulation. For example, in case P01 the critical thresholds identified for FIS and VR were reached at 10 000 N after 29 and 31 substeps, respectively, while the simulation would stop due to numerical instabilities after 44 substeps. On average, this mechanism would save about 20 % of iterations, ultimately resulting in an even higher computational time saving, as disk I/O of the cumulative results dominate the actual FE simulation time after many iterations.

### 3.3. Preliminary push out test results

Due to the high computational costs of the procedure, the primary stability of the implant was checked using the push-out test only for one patient (P04). At the initial load step (*i.e.*, before applying any compressive load) and after the first hammering stroke ($F = 1000$ N), the push-out simulation showed convergence problems due to stem rigid body motion. As we increased the compressive load (*i.e.*, from $F = 2000$ N on), the stability of the stem increased, leading to a reduction in the displacement during the push-out (Fig 7a). However, as damage continued to be accumulated within the structure, the displacement increased until it reached again stem rigid-body motion. The same phenomenon is illustrated in Fig. 7b, showing the trend of push-out stiffness throughout the simulation (with a reversed trend, as defined in Eq (8)). In the same graph, the trend of FIS during the simulation is also shown. It can be observed that, in correspondence of the rapid decrease in push-out stiffness (last load step), the Fracture Internal Surface increased dramatically. Notably, at the time this sharp slope change was observed in both quantities, the FIS value was approximately 1300 mm², which aligns with the proposed threshold.

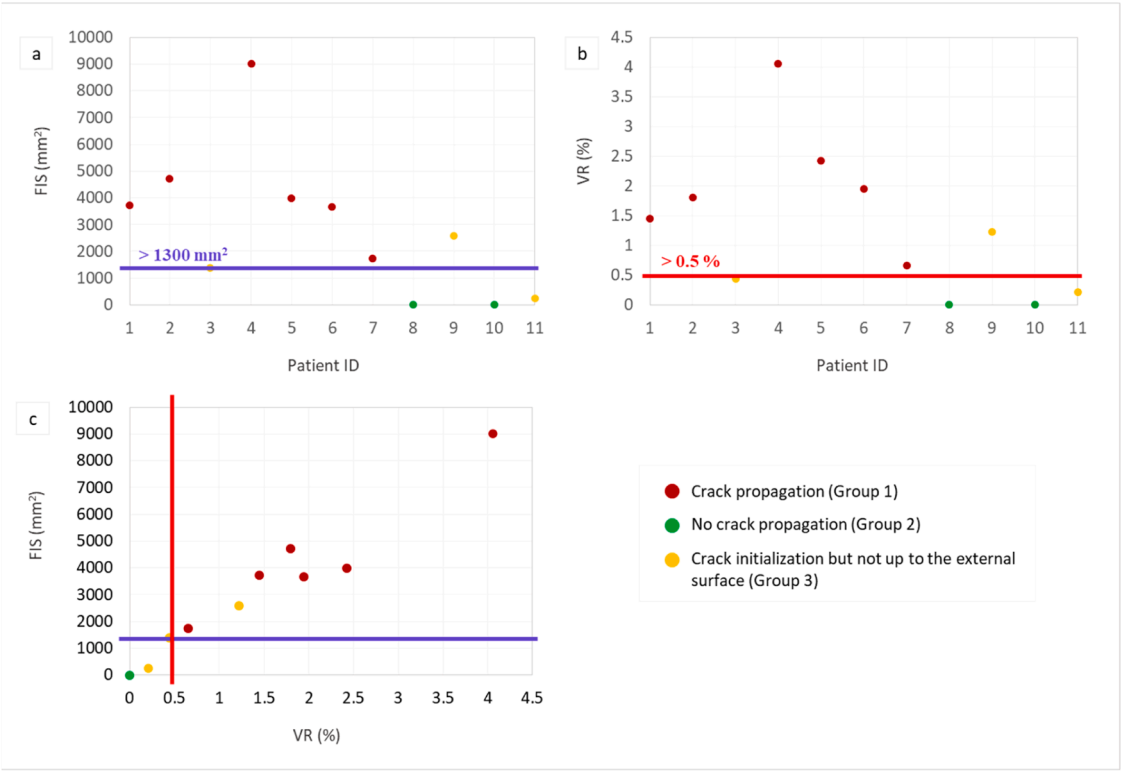


**Fig. 6.** Fracture Internal Surface (a) and Volume Ratio (b) plotted for the 11 simulated patients; in purple (a) and in red (b) the respective threshold values, identified from an empirical analysis of the results; c) Fracture Internal Surface plotted against Volume Ratio for each simulated patient.

**Table 3**
Simulation substeps in the last load step using different stopping criteria. Only patients of groups 1 and 3 are reported. Patient P11 did not show numerical instability up to the maximum applied load.

| Patient | # Substeps (FIS criterion) | # Substeps (VR criterion) | # Substeps (num instab) |
|---|---|---|---|
| **P01** | 29 | 31 | 44 |
| **P02** | 27 | 29 | 35 |
| **P03** | 2 | Never | 2 |
| **P04** | 14 | 16 | 28 |
| **P05** | 13 | 8 | 22 |
| **P06** | 9 | 9 | 19 |
| **P07** | 1 | 1 | 1 |
| **P09** | 10 | 8 | 40 |
| **P11** | Never | Never | N.A. |

### *3.4. Effect of the elastic modulus variation on the simulation results*

The elastic modulus variation did not lead to a notable difference in the results; as shown in Table 4, only two patients among all the simulated femurs had lower failure loads (P07, P09) when decreasing the elastic modulus by 3 %. However, only patient P07 still had a last applied load below the maximum value of a hammer blow.

## 4. Discussion

This study aimed to describe a new approach to simulate intra-operative fractures in cementless hip designs and quantify the damage. A mock stem design was used to demonstrate the feasibility of simulating the crack formation and propagation and estimating the load that would cause an IFF at reasonable computational costs (some hours per model). The novel approach was tested on eleven patients selected by

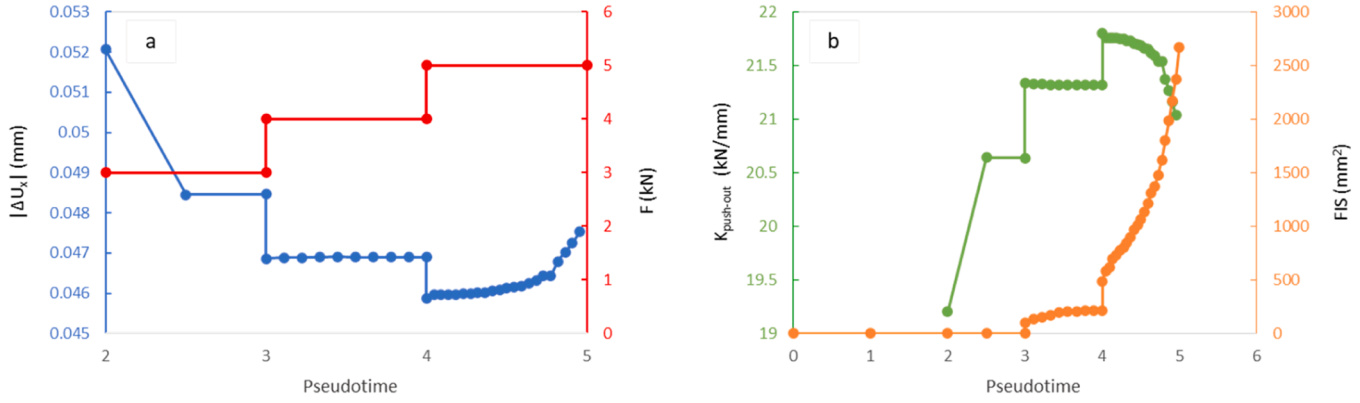


**Fig. 7.** a) Relative displacement of the node where the load was applied during the push-out test (in blue) plotted against pseudotime. The compressive load applied is also depicted in the graph (in red). b) Push-out stiffness (in green) and Fracture Internal Surface (in orange) curves plotted against pseudotime.

**Table 4**
Failure load values for the eleven patients simulated by varying the elastic modulus of the femur by +/- 3 %. "N.A." was used for the models in which a higher value of E was not considered for the simulations, as these models were not fractured with a force greater than 10 000 N using the nominal value of E.

| Patient | Failure load (N) *E* nominal | Failure load (N) *E* −3 % | Failure load (N) *E* + 3 % |
|---|---|---|---|
| **P01** | 10 000 | = | = |
| **P02** | 9000 | = | ↑ 10 000 |
| **P03** | 7000 | = | = |
| **P04** | 5000 | = | = |
| **P05** | 9000 | = | = |
| **P06** | 5000 | = | = |
| **P07** | 3000 | ↓ 2000 | 3000 |
| **P08** | >10 000 | = | N.A. |
| **P09** | 7000 | ↓ 6000 | 7000 |
| **P10** | >10 000 | = | N.A. |
| **P11** | >10 000 | = | N.A. |

age, gender, and femur length to consider population anatomo-densitometric variability. Two possible damage quantifier were explored to determine when the IFF would occur, evaluating i) the fracture internal surface, and ii) the volume ratio of the killed elements. Also, an additional preliminary analysis was performed to assess the primary stability of the implant during insertion, simulating a push-out test. From the analysis of the results, all methods were found to be consistent in term of fracture load values. The instant the push-out curve changed trend (*i.e.*, the displacement started to increase) was quite similar to the one identified with the other two damage quantification criteria candidates. Using the fracture internal surface or the volume ratio as irreversible damage thresholds, the simulation would have been interrupted at the same load step, so with a failure load equal to that obtained with excessive distortion elements criterion, but performing fewer load steps during the last constant phase (as reported in Table 3), ultimately reducing the computational cost. Although the push-out test can be considered the closest representation to reality to assess the stability of the implant, its implementation requires very high computational costs (a day or more). Considering the robustness and lower computational expense of the other two criteria, the idea is to primarily use one of these, resorting to push-out simulation only for borderline cases. However, to proceed in this direction, it is essential to verify that the threshold values, chosen after an empirical analysis of the simulated model results, robustly identify the moment when the structure stability is irreversibly impaired. Therefore, testing and validating these threshold values across more cases (also with physical experimental setups), while carefully considering model prediction uncertainties, becomes crucial.

Although our study primarily focused on the methodology for simulating crack propagation and identifying criteria to quantify damage, some considerations can be made regarding potential critical cases in which the femur could be at high risk of fracture during implant insertion. For example, if we look at Table 2 and the results reported in the damage quantification section, we observe that the same failure load is obtained when considering different criteria (*i.e.*, when the critical thresholds identified for the FIS and VR criteria were reached, as well as when considering only numerical instabilities) and these failure loads are all above the values typically observed during surgical hammering, except for P07, which exceeded FIS and VR values of 1300 $mm^2$ and 0.5 % under a compressive load of 3000 N. Therefore, this single case could be considered a femur at high risk of fracture. Notably, patient P07 has a very low (the lowest in the cohort) bone mineralization, being a female with a T-score of −2.31 (corresponding to an areal bone mineral density of 0.660 $g/cm^2$), indicating high fragility due to osteoporosis (Table 1).

This study has some limitations. A first critical point concerns the use of a quasi-static model, although the stem insertion is a dynamic process. Even though this approach is less accurate compared to methods based on transient analysis solved with an explicit time integration scheme [14,15] or those explicitly modelling fracture mechanics, it is computationally more efficient and could be employed to estimate the risk of IFF across hundreds of patient-surgery combinations. Additionally, considering the low strain rates involved, *i.e.*, rarely above 1 % per second, Titanium alloy does not show a viscous behaviour, and the change in bone apparent modulus is minimal [38]. Another noteworthy limitation concerns the modelling approach employed for the reaming procedure. In surgical practice, the bone is typically trimmed with a rasp from the smallest size to the one to be implanted, resulting in a hole slightly smaller than the stem section. In our FE models, an idealized Boolean subtraction was performed between the bone and the rasp of the nominal size. To the authors' knowledge, the use of Boolean subtraction, which assumes a perfect reamed cavity, is common practice in the literature for reproducing prosthesis implantation in FE models [18,39]. Regarding the virtual surgery performed, an ideal surgical outcome was assumed for all eleven post-operative femoral anatomies. It is important to note that, according to previous works of our group on the reproducibility of pre-operative planning [40] and the differences between the planned and the surgically achieved pose [41], this assumption may not always be true. In a follow-up study it would be interesting to introduce stem size uncertainty and varus-valgus and add-abduction angular uncertainty in the pose of the stem inside the femur.

If we wanted to compare the obtained results with the ones present in the literature, in which crack propagation during stem insertion was simulated with a quasi-static procedure and elements deactivation, this could be difficult. To the authors' best knowledge, no other work developed with our approach has been reported. Regarding the final load values, *i.e.*, the ultimate load at which the crack reached the surface, they seem to be in accordance with the ones obtained by Hennicke et al. [39] in a recent work about the subject-specific FE modelling of periprosthetic femoral fractures due to stumbling, in which failure loads were found to be around 4000–5000 N. Moreover, the location of the fractures obtained seems to agree with the Vancouver Classification proposed by Masri et al. [42], which allows grading the intraoperative fractures considering three key factors: location, stability of the implant, and the surrounding bone stock [18]. When comparing the results from our FE models with the Vancouver Classification, it is of particular interest the fact that the fracture pattern matched closely with type B2, which is characterised by a fracture located at the level of the prosthetic stem and by a stable implant (*i.e.*, a nondisplaced crack). In these cases, nondisplaced linear cracks usually occur during broach or implant insertion because of the increased hoop stresses on the bone during device insertion. Given its stability, many of these fractures are not recognised intraoperatively and can only be observed on a postoperative radiograph [43].

In conclusion, a pipeline to simulate crack propagation during femoral stem insertion was proposed in this work. The results obtained from analysing the simulation in terms of damage quantification and failure load demonstrated that the proposed criteria can efficiently predict implant instability as the fracture propagates. The findings of this study represent a starting point for future investigations to further validate the proposed damage quantification criteria and estimate the risk of intraoperative femoral fractures (IFF) for new stem designs.

## Open access data

The Open Access data associated to this paper can be found on the UNIBO institutional repository, at this DOI: https://doi.org/10.6092/unibo/amsacta/8058.

## Funding

This study was supported by the European Commission through the H2020 projects "CompBioMed2: A Centre of Excellence in Computational Biomedicine" (topic INFRAEDI-02-2018, grant ID 823712) and "In Silico World: Lowering barriers to ubiquitous adoption of In Silico

Trials" (topic SC1-DTH-06-2020, grant ID 101016503). We acknowledge PRACE for awarding access to the Fenix Infrastructure resources at CINECA, partially funded by the European Union's Horizon 2020 research and innovation programme through the ICEI project under grant agreement No. 800858.

## Ethical approval

Work on human beings that is submitted to *Medical Engineering & Physics* should comply with the principles laid down in the Declaration of Helsinki; Recommendations guiding physicians in biomedical research involving human subjects. Adopted by the 18th World Medical Assembly, Helsinki, Finland, June 1964, amended by the 29th World Medical Assembly, Tokyo, Japan, October 1975, the 35th World Medical Assembly, Venice, Italy, October 1983, and the 41st World Medical Assembly, Hong Kong, September 1989. The study was approved by the local ethical committee (CE AVEC 731/202/Oss/IOR, 04 August 2020).

## Declaration of competing interest

The authors declare that they do not have any financial or personal relationships with other people or organisations that could have inappropriately influenced this study.

## References

[1] Viceconti M, Affatato S, Baleani M, Bordini B, Cristofolini L, Taddei F. Pre-clinical validation of joint prostheses: a systematic approach. J Mech Behav Biomed Mater Jan. 2009;2(1):120–7. https://doi.org/10.1016/j.jmbbm.2008.02.005.

[2] Abdel MP, Watts CD, Houdek MT, Lewallen DG, Berry DJ. Epidemiology of periprosthetic fracture of the femur in 32 644 primary total hip arthroplasties: a 40-year experience. Bone Jt J Apr. 2016;98-B(4):461–7. https://doi.org/10.1302/0301-620X.98B4.37201.

[3] Ioannidis CC, Dabirrahmani D, Li Q, Zhang ZP, Chen JN, Appleyard R. Impaction Loads Resulting in Intraoperative Periprosthetic Femoral Fracture: a Finite Element Study. Appl Mech Mater May 2014;553:299–304. https://doi.org/10.4028/www.scientific.net/AMM.553.299.

[4] 'Italian Arthoprosthesis Registry Riap annual report 2020'. [Online]. Available: http://riap.iss.it/riap/it/attivita/report.

[5] Evans JT, Evans JP, Walker RW, Blom AW, Whitehouse MR, Sayers A. How long does a hip replacement last? A systematic review and meta-analysis of case series and national registry reports with more than 15 years of follow-up. The Lancet Feb. 2019;393(10172):647–54. https://doi.org/10.1016/S0140-6736(18)31665-9.

[6] Rutenberg TF, et al. Relatively High Complication and Revision Rates of the Mayo ® Metaphysical Conservative Femoral Stem in Young Patients. Orthopedics Jul. 2018;41(4). https://doi.org/10.3928/01477447-20180503-01.

[7] Timmer C, Gerhardt DMJM, de Visser E, de Kleuver M, van Susante JLC. High incidence of intraoperative calcar fractures with the cementless CLS Spotorno stem. Eur J Orthop Surg Traumatol Oct. 2018;28(7):1291–6. https://doi.org/10.1007/s00590-018-2217-8.

[8] Arnholdt J, et al. The Mayo conservative hip: complication analysis and management of the first 41 cases performed at a University level 1 department. BMC Musculoskelet Disord Dec. 2017;18(1):250. https://doi.org/10.1186/s12891-017-1613-2.

[9] Sakai R, et al. Hammering Force during Cementless Total Hip Arthroplasty and Risk of Microfracture. HIP Int May 2011;21(3):330–5. https://doi.org/10.5301/hip.2011.8408.

[10] Sakai R, et al. Hammering Sound Frequency Analysis and Prevention of Intraoperative Periprosthetic Fractures during Total Hip Arthroplasty. HIP Int Nov. 2011;21(6):718–23. https://doi.org/10.5301/HIP.2011.8823.

[11] Dubory A, Rosi G, Tijou A, Lomami HA, Flouzat-Lachaniette C-H, Haïat G. A cadaveric validation of a method based on impact analysis to monitor the femoral stem insertion. J Mech Behav Biomed Mater Mar. 2020;103:103535. https://doi.org/10.1016/j.jmbbm.2019.103535.

[12] Pastrav LC, Jaecques SVN, Mulier M. Determination of Total Hip Replacement stem insertion endpoint and stability assessment by vibration analysis: first experiences with per-operative measurements. Proceeding ISMA 2006:12.

[13] Tijou A, et al. Monitoring cementless femoral stem insertion by impact analyses: an *in vitro* study. J Mech Behav Biomed Mater Dec. 2018;88:102–8. https://doi.org/10.1016/j.jmbbm.2018.08.009.

[14] A. Ag, P. Lc, and J. Svn, 'Intraoperative manufactured hip prosthesis insertion - a finite element simulation', p. 2.

[15] Monea AG, Pastrav LC, Mulier M, Van der Perre G, Jaecques SV. Numerical simulation of the insertion process of an uncemented hip prosthesis in order to evaluate the influence of residual stress and contact distribution on the stem initial stability. Comput Methods Biomech Biomed Engin Feb. 2014;17(3):263–76. https://doi.org/10.1080/10255842.2012.681644.

[16] Bessho M, et al. Prediction of the strength and fracture location of the femoral neck by CT-based finite-element method: a preliminary study on patients with hip fracture. J Orthop Sci Nov. 2004;9(6):545–50. https://doi.org/10.1007/s00776-004-0824-1.

[17] Saemann M, Darowski M, Bader R, Sander M, Kluess D. In: Experimental validation of a finite element model of periprosthetic femoral fracture in a stumbling scenario', presented at the 26th Congress of the European Society of Biomechanics, Milan, Italy; Jul. 2021.

[18] Miles Brad, et al. Subject specific finite element modeling of periprosthetic femoral fracture using element deactivation to simulate bone failure. Med Eng Phys 2015. https://doi.org/10.1016/j.medengphy.2015.03.012.

[19] Marco Miguel, Giner Eugenio, Larrainzar-Garijo Ricardo, Caeiro José Ramón, Miguélez María Henar. Modelling of femur fracture using finite element procedures. Eng Fract Mech 2018. https://doi.org/10.1016/j.engfracmech.2018.04.024.

[20] Cui Y, et al. Incremental Element Deletion-Based Finite Element Analysis of the Effects of Impact Speeds, Fall Postures, and Cortical Thicknesses on Femur Fracture. Materials (Basel) Apr. 2022;15(8):2878. https://doi.org/10.3390/ma15082878.

[21] Cann CE, Adams JE, Brown JK, Brett AD. CTXA Hip—An Extension of Classical DXA Measurements Using Quantitative CT. PLoS ONE Mar. 2014;9(3):e91904. https://doi.org/10.1371/journal.pone.0091904.

[22] Looker AC, et al. Updated Data on Proximal Femur Bone Mineral Levels of US Adults. Osteoporos Int Aug. 1998;8(5):468–90. https://doi.org/10.1007/s001980050093.

[23] Paggiosi MA, et al. International variation in proximal femur bone mineral density. Osteoporos Int Feb. 2011;22(2):721–9. https://doi.org/10.1007/s00198-010-1336-9.

[24] Qiao Li, 'Modelling the femur strength in a virtual postmenopausal osteoporotic population for application to in silico clinical trials', PhD thesis, University of Sheffield, 2021. [Online]. Available: https://etheses.whiterose.ac.uk/31196/.

[25] *GrabCAD*. (Jun. 01, 2020). [Online]. Available: hip - Recent models | 3D CAD Model Collection | GrabCAD Community Library.

[26] P. Cignoni, M. Callieri, M. Corsini, M. Dellepiane, F. Ganovelli, and G. Ranzuglia, 'MeshLab: an Open-Source Mesh Processing Tool', p. 8, [Online]. Available: https://www.meshlab.net/.

[27] Viceconti M, et al. CT-based surgical planning software improves the accuracy of total hip replacement preoperative planning. Med Eng Phys Jun. 2003;25(5):371–7. https://doi.org/10.1016/S1350-4533(03)00018-3.

[28] Eberle S, Göttlinger M, Augat P. An investigation to determine if a single validated density–elasticity relationship can be used for subject specific finite element analyses of human long bones. Med Eng Phys Jul. 2013;35(7):875–83. https://doi.org/10.1016/j.medengphy.2012.08.022.

[29] Altai Z, Qasim M, Li X, Viceconti M. The effect of boundary and loading conditions on patient classification using finite element predicted risk of fracture. Clin Biomech Aug. 2019;68:137–43. https://doi.org/10.1016/j.clinbiomech.2019.06.004.

[30] Qasim M, et al. Patient-specific finite element estimated femur strength as a predictor of the risk of hip fracture: the effect of methodological determinants. Osteoporos Int Sep. 2016;27(9):2815–22. https://doi.org/10.1007/s00198-016-3597-4.

[31] Schileo E, et al. An accurate estimation of bone density improves the accuracy of subject-specific finite element models. J Biomech Aug. 2008;41(11):2483–91. https://doi.org/10.1016/j.jbiomech.2008.05.017.

[32] Taddei F, Schileo E, Helgason B, Cristofolini L, Viceconti M. The material mapping strategy influences the accuracy of CT-based finite element models of bones: an evaluation against experimental measurements. Med Eng Phys Nov. 2007;29(9):973–9. https://doi.org/10.1016/j.medengphy.2006.10.014.

[33] Morgan EF, Bayraktar HH, Keaveny TM. Trabecular bone modulus–density relationships depend on anatomic site. J Biomech Jul. 2003;36(7):897–904. https://doi.org/10.1016/S0021-9290(03)00071-X.

[34] Reggiani B, Cristofolini L, Varini E, Viceconti M. Predicting the subject-specific primary stability of cementless implants during pre-operative planning: preliminary validation of subject-specific finite-element models. J Biomech Jan. 2007;40(11):2552–8. https://doi.org/10.1016/j.jbiomech.2006.10.042.

[35] Poelert S, Valstar E, Weinans H, Zadpoor AA. Patient-specific finite element modeling of bones. Proc Inst Mech Eng Apr. 2013;227(4):464–78. https://doi.org/10.1177/0954411912467884.

[36] Schileo E, Taddei F, Cristofolini L, Viceconti M. Subject-specific finite element models implementing a maximum principal strain criterion are able to estimate failure risk and fracture location on human femurs tested *in vitro*. J Biomech Jan. 2008;41(2):356–67. https://doi.org/10.1016/j.jbiomech.2007.09.009.

[37] Bonfield W. Advances in the fracture mechanics of cortical bone. J Biomech Jan. 1987;20(11–12):1071–81. https://doi.org/10.1016/0021-9290(87)90025-X.

[38] Hansen U, Zioupos P, Simpson R, Currey JD, Hynd D. The Effect of Strain Rate on the Mechanical Properties of Human Cortical Bone. J Biomech Eng Feb. 2008;130(1):011011. https://doi.org/10.1115/1.2838032.

[39] Hennicke NS, Saemann M, Kluess D, Bader R, Sander M. Subject specific finite element modelling of periprosthetic femoral fractures in different load cases. J Mech Behav Biomed Mater Dec. 2021;126:105059. https://doi.org/10.1016/j.jmbbm.2021.105059.

[40] Viceconti M, Lattanzi R, Zannoni C, Cappello A. Effect of display modality on spatial accuracy of orthopaedic surgery pre-operative planning applications. Med Inform Internet Med Jan. 2002;27(1):21–32. https://doi.org/10.1080/14639230110110233.

[41] Popescu F, Viceconti M, Grazi E, Cappello A. A new method to compare planned and achieved position of an orthopaedic implant. Comput Methods Programs Biomed Jun. 2003;71(2):117–27. https://doi.org/10.1016/S0169-2607(02)00091-3.

[42] Masri BA, Meek RMD, Duncan CP. Periprosthetic Fractures Evaluation and Treatment. Clin Orthop Mar. 2004;420:80–95. https://doi.org/10.1097/00003086-200403000-00012.

[43] Davidson D, Pike J, Garbuz D, Duncan CP, Masri BA. Intraoperative Periprosthetic Fractures During Total Hip Arthroplasty: evaluation and Management. J Bone Jt Surg-Am Sep. 2008;90(9):2000–12. https://doi.org/10.2106/JBJS.H.00331.